PAPER • OPEN ACCESS

Experimental realization of smectic phase in vortex matter induced by symmetric potentials arranged in two-fold symmetry arrays

New Journal of Physics
The open access journal at the forefront of physics

Deutsche Physikalische Gesellschaft DPG
IOP Institute of Physics

Published in partnership with: Deutsche Physikalische Gesellschaft and the Institute of Physics

OPEN ACCESS

RECEIVED
13 April 2015

REVISED
14 August 2015

ACCEPTED FOR PUBLICATION
17 August 2015

PUBLISHED
14 September 2015

PAPER

Experimental realization of smectic phase in vortex matter induced by symmetric potentials arranged in two-fold symmetry arrays

J del Valle[1], A Gomez[1], E M Gonzalez[1,2], M R Osorio[2], F Galvez[1], D Granados[2] and J L Vicent[1,2]

[1] Departamento Fisica de Materiales, Facultad de Ciencias Fisicas, Universidad Complutense, 28040 Madrid, Spain
[2] IMDEA-Nanociencia, Cantoblanco, 28049 Madrid, Spain

Keywords: phase transition, superconductivity, nanostructures

Abstract

Smectic order has been generated in superconducting Nb films with two-fold symmetry arrays of symmetric pinning centers. Magnetic fields applied perpendicularly to the films develop a vortex matter smectic phase that is easily detected when the vortices are commensurate with the pinning center array. The smectic phase can be turned on and off with external parameters.

1. Introduction

Crystals exhibit fully translational periodicity; on the other hand, liquids do not show translational periodicity at all. In between, the smectic phase shows translation periodicity only in one dimension. Smectic systems are solid-like in one direction and liquid-like in two directions. Liquid crystals are the paradigm of smectic phases, but we have to notice that these phases show up in many systems other than liquid crystals. In addition, smectic order is claimed to be the clue to understanding many phenomena occurring in different systems. Examples, taken from very dissimilar systems, are nanorods with smectic order into patterned plasmonic nanostructures [1], smectic modulations in the pseudogap states of underdoped $Bi_2Sr_2CaCu_2O_{8+\delta}$ superconductors [2] and spontaneous ferroelectric order in a bent-core smectic liquid crystal [3]. Smectic order has been of interest outside the liquid crystal framework; for example, de Gennes has explored the possible analogy between the smectic phase and the mixed state phase in superconductors [4]. Carlson *et al* examined the possibility of a smectic phase in anisotropic superconductors [5], and Reichhardt *et al* [6] showed that quenched disorder can induce a smectic phase. One promising system in which to look for smectic phases is vortices in layered superconductors. Vortex matter is a very well established field, making it an ideal playground to test different models and go deeper into relevant features associated with phase transitions and related topics such as vortex lattice dynamics [7–12]. Among layered systems, superconducting dichalcogenides [13–15], cuprates [16–18] and pnictides [19–21] have drawn the attention of many researchers. After a pioneer work [22] and some debate concerning the development of smectic order in vortex matter [23, 24], smectic phases were experimentally found in cuprates [25] and in dichalcogenides [26].

In this paper, we show how to induce a vortex matter smectic phase in non-layered superconductors with a periodic array of symmetric pinning potentials, and how this vortex matter phase can be easily handled.

2. Experimental results

In layered superconductors the layers help to induce smectic order. Non-layered superconductors lack a suitable structure that can promote a smectic order. In layered materials, a magnetic field applied parallel to the layers can trigger a smectic phase [26, 27]. Layers allow placing and controlling the vortices easily. In the present work we dealt with plain superconductors (Nb films), so a different approach is needed. First, we need controlling vortices in plain superconductors. Arrays of non-superconducting centers embedded in the superconducting films are a suitable way to accomplish this aim. Many researchers have studied vortices in superconducting films with artificially periodic pinning centers [28–33]. Superconducting films with periodic pinning nanocenter arrays show noteworthy effects when matching between the vortex lattice and the array unit cell occurs. Under

matching conditions magnetoresistance shows minima. These minima show strong reduction of the dissipation, and two neighboring minima are always separated by the same magnetic field value. The first minimum appears at magnetic field $H_1 = (\Phi_0/S)$, where S is the unit cell area of the pinning array and $\Phi_0 = 2.07\,10^{-15}$ Wb is the quantum fluxoid. Other minima appear at commensurability fields $H_n = n(\Phi_0/S)$, where $n > 1$ is an integer. Minima can be also observed at fractional matching fields $H_f = f(\Phi_0/S)$, where f is a non-integer number. So, under matching conditions between the array and the vortex lattice, we are able to control the superconducting vortices. All the data presented in this work were recorded with the magnetic field applied perpendicular to the film and with magnetic field values that fulfill the commensurability constraint, i.e. the applied field is a fraction or multiple of the first matching field. Note that vortex behavior is governed by the interplay between random intrinsic pinning, which is known to be strong in Nb thin films [34], and artificially induced periodic potentials [35, 36]. As explained by Pogosov *et al* [37], under matching conditions, both these factors affect the system. Competition between these two pinning forces and elastic strains lead to the appearance of defects in the vortex lattice, which break the long-range translational symmetry, making the correlation length finite [38]. Therefore, a perfect ordered vortex lattice is absent.

In this work, the samples are 100 nm-thick Nb films grown by sputtering on top of arrays of Cu dots (220 nm diameter and 40 nm thickness) which were fabricated on a Si substrate by sputtering and electron beam lithography techniques. These nanodot dimensions yield a filling factor of a single vortex trapped for nanodots [39]. Finally, the samples are patterned in a cross-shaped bridge for magnetotransport measurements. (For experimental details, see [39]). To study the vortex phases in this type of samples we have followed the approach reported in [40–42]; the seminal paper of Fisher *et al* [40] about glass-to-liquid second-order phase transition and how to extract the critical exponents; the work of Strachan *et al* [41] regarding a careful and unambiguous method to determine the critical temperatures; and the work of Villegas *et al* [42] on periodic pinning and vortex glass phases. Using a scaling analysis of I-V characteristics, Villegas *et al* found that Nb thin films with periodic arrays of pinning centers show a continuous glass transition, similar to that observed in plain Nb films. The random and periodic pinning mechanisms compete and yield a glass phase that does not present long-range topological order.

We have grown a sample with an array of 400 $\times$ 400 nm^2 unit cells (SQ-sample in the following), that we use as the standard sample for our study. We have measured (I, V) curves at several matching fields. The results do not depend on the value of the matching field. Figure 1(a) shows I-V isotherms at $H = 3H_1$ (H_1 being the value of the first matching field $H_1 = \Phi_0/a^2$, with $\Phi_0 = 2.07$ 10-15 Wb and $a = 400$ nm). As $I \rightarrow 0$, two different trends are observed. Isotherms close to T_c show a linear dependence $V \propto I$; this ohmic behavior corresponds to the vortex liquid phase. However, for lower temperatures I-V curves become highly nonlinear for vanishing current, and voltage drops abruptly. This change corresponds to a transition to a non-dissipative vortex glass state. This melting transition is continuous, so we can define critical exponents ν and z at which the phase correlation length of the glass $\xi_g \sim (T–T_g)^{-\nu}$ and the relaxation time $\tau_g \sim \xi_g^z$ diverge at the transition, T_g being the melting temperature. Following [40], I-V data can be scaled down into two single curves according to:

$$\rho\left(1–T/T_g\right)^{\nu(D-2-z)} = f_{\pm}\left\{(J/T)\left(1–T/T_g\right)^{\nu(1-D)}\right\} \quad (1)$$

where D is the dimensionality of the system, ν and z are the static and dynamic critical exponents respectively, and $f_{\pm}$ are two scaling functions above and below T_g. Figure 1(b) shows scaling behavior for sample SQ at $H = 3H_1$. Critical exponents $\nu = 1.0 \pm 0.1$ and $z = 6.7 \pm 0.2$ are obtained, in the range expected by the theory: $\nu \approx$ 1-2 and $z \approx$ 4-7. The dimensionality of the system is D = 3.

In summary, we have found successful scaling analysis of the I-V data for sample SQ for magnetic fields which correspond to different matching fields, obtaining ν and z values in the ranges ($1 \pm 0.1, 1.1 \pm 0.1$) and ($6.5 \pm 0.2, 6.7 \pm 0.2$) respectively, supporting evidence of vortex glass to liquid transition in all cases, as expected.

Following Strachan *et al* [41], the inset in figure 1(b) shows the derivatives of log(V)-log(I) curves. We clearly observe the transition from ohmic to nonlinear behavior at low currents. This crossover takes place at T_g, allowing us to determine the melting temperature using a direct and independent method, with an error of $\pm$5 mK.

Once we have established the frame of our study, the symmetry of the array is lowered from four-fold to two-fold symmetry. We have fabricated two samples, one with array unit cell 400 $\times$ 600 nm^2 (R46 sample) and the other with array unit cell 400 $\times$ 800 nm^2 (R48 sample). The rectangular pinning landscape induces a strong anisotropic behavior in the vortex dynamics, as reported by Velez *et al* [43]. This anisotropic effect can be explored by (I, V) isotherm data taken with vortices moving along the short and long sides of the rectangular unit cell. Several (I, V) curves were measured at different matching fields. Figures 2(a) and (b) show the (I, V) isotherm curves measured along the short and long sides of the rectangular unit cell for the first matching field. The analysis of these raw data, following the same procedure as in the SQ sample, leads to the following

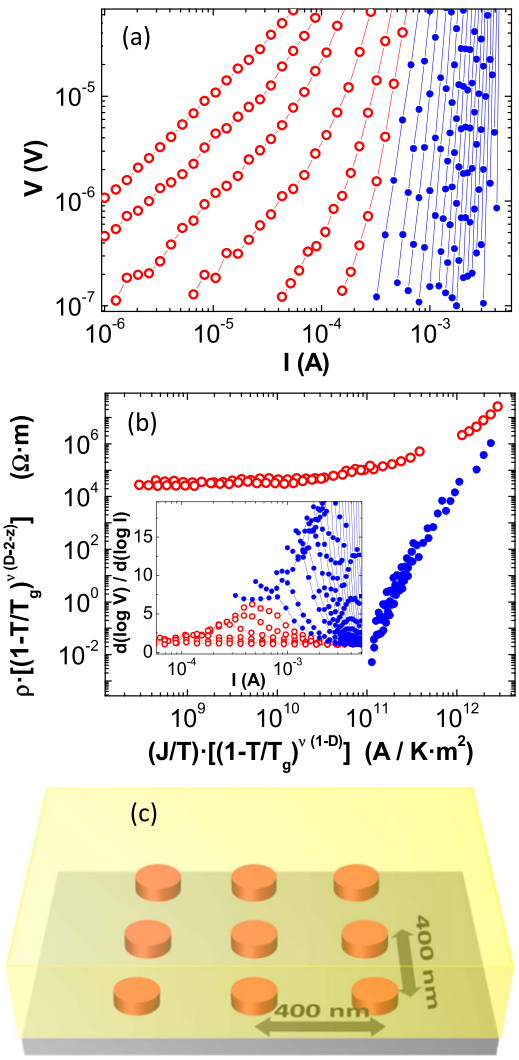

Figure 1. (a) *I-V* isotherms from 0.969 T_c to 0.997 T_c, data taken every 10 mK, for sample SQ ($T_c = 8.0$ K) and $H = 380$ Oe ($H = 3H_1$). Isotherms above T_g shown as open red circles and below T_g as blue dots. (b) Scaling of the *I-V* data into two curves corresponding to the vortex liquid (red hollow dots) and glass (blue dots) phases. Derivatives of the log (*V*)—log (*I*) curves as a function of the current are plotted in the inset. $T_g = 0.989T_c$, as well as critical exponents $\nu = 1.0$ and $z = 6.7$, are obtained (see text). (c) Sketch of sample SQ: array of Cu dots with 400 × 400 nm^2 unit cell embedded in Nb film grown on Si substrate. (Sketch is not to scale).

remarkable experimental facts in the low matching field regime: (i) the experimental data cannot be scaled down, (ii) using the log(*V*)-log(*I*) derivative analysis, two different values for T_g (T_{gs} and T_{gl} in the following) are obtained. T_{gs} is the transition temperature found for vortices moving along the short side of the array unit cell, and T_{gl} is the transition temperature obtained for vortices moving along the long side of the array unit cell.

This implies that for $T_{gs} < T < T_{gl}$, the low current behavior of the *I-V* curves is ohmic along one direction and nonlinear along the other, so the system shows liquid or glass vortex dynamics depending on the direction.

3. Discussion

This behavior suggests that in between these two temperatures (T_{gs}, T_{gl}) vortex matter is in a smectic phase. The important feature of the smectic phase, which distinguishes it from the nematic phase, is that vortices are arranged in rows. This fact leads to two melting temperatures, ruling out a nematic phase. The melting from glass to liquid only occurs along vortex motion parallel to the short side. Figure 3(a) shows the potential landscape, which helps to visualize the translation periodicity along the long side. This landscape is obtained taking into account that vortices move in the potential centers which are induced by the Cu nanodot arrays; i.e. the vortices have to probe the structure of the pinning array close to T_c. This vortex-nanodot interaction can be roughly estimated considering the volume of the vortex core within the nanodot volume, following Campbell and Evetts [44]. In this approach the coherence length ξ plays the leading role in the interaction between the

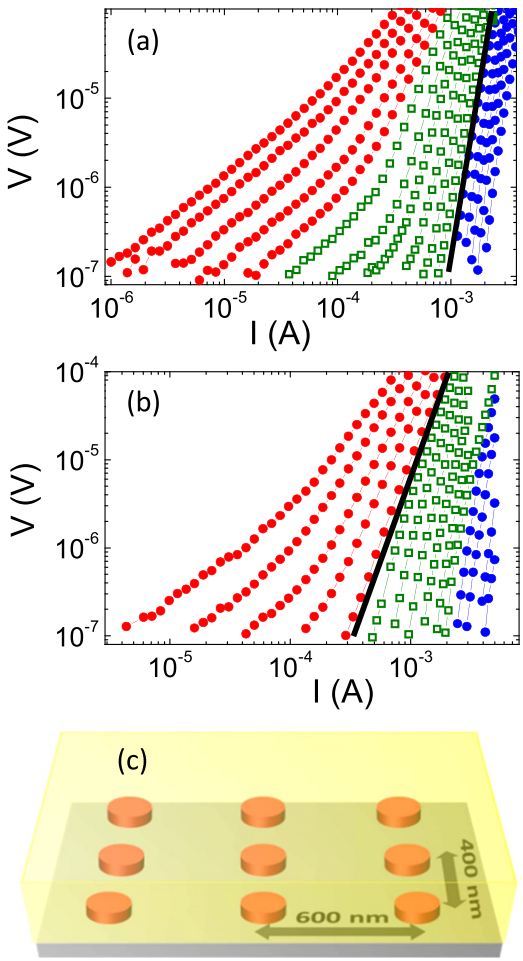

Figure 2. *I-V* isotherms for sample R46 ($T_c = 8.7$ K), from $0.978T_c$ to $0.995T_c$, data taken every 10 mK with $H = 86$ Oe ($H = H_1$) for vortices moving (a) along the short and (b) along the long sides of the rectangular unit cell respectively. Depending on the direction, two different T_g (solid lines) are obtained (see text): $T_{g,s} = 0.983T_c$ and $T_{g,l} = 0.990T_c$, with a 60 mK difference between both temperatures (green hollow squares) which spans the vortex glass (blue dots) and vortex liquid (red dots). (c) Sketch of sample R46: array of Cu dots with 400×600 nm^2 unit cell embedded in Nb film grown on Si substrate. (Sketch is not to scale).

vortex core and the non-magnetic pinning centers (Cu nanodots in our case). The estimation of the vortex core is obtained from the Ginzburg-Landau coherence lengths, which are extracted as usual from $H_{c2}(T)$ measurements. Figure 3(a) shows a plot of this interaction potential when temperature is close to T_c and therefore the coherence length ξ is large. Interestingly, when the temperature decreases, diminishing the coherence length, the overlapping potential, which mimics a layered structure, vanishes and the potential finally recaptures the pinning landscape induced by the array of nanodots, as shown in figure 3(b). It is worth pointing out that this temperature interval comprises the smectic region. These potentials are the background of the liquid-like behavior, while the periodicity of the overlapping potentials supports the solid-like behavior in the perpendicular direction.

The difference between the two melting temperatures T_{gs} and T_{gl} is 60 mK at the first matching field, the low T_{gs} being the value obtained when the vortices move along the short side of the array unit cell. This temperature difference diminishes as the applied magnetic fields increase. Scaling down the experimental data is only possible when the two T_g merge and a vortex glass–to–vortex liquid transition is recovered with usual values of the critical exponents; for example, the critical exponents for $H = 5H_1$ are $\nu = 1.0 \pm 0.1$, and $z = 6.6 \pm 0.2$. See figure 3(c) for a complete phase diagram picture.

We have also measured (I, V) curves for several matching fields in sample R48, in which the long side of the array unit cell (800 nm) is twice as long as the short side (400 nm). Figure 4 shows the (I, V) raw data for the first matching field. As in sample 46, for the first matching field (H_1) in sample R48, the experimental data cannot be scaled down and two T_g are obtained. In this case the temperature difference is 250 mK, more than four times the value found in sample R46 (60 mK). Scaling down the experimental data is only possible when the two T_g merge, but in sample R48 the critical exponents depend on the vortex motion direction in the whole range that we have measured. For instance for $17H_1$, the critical exponents extracted from the scaling for vortex motion along the

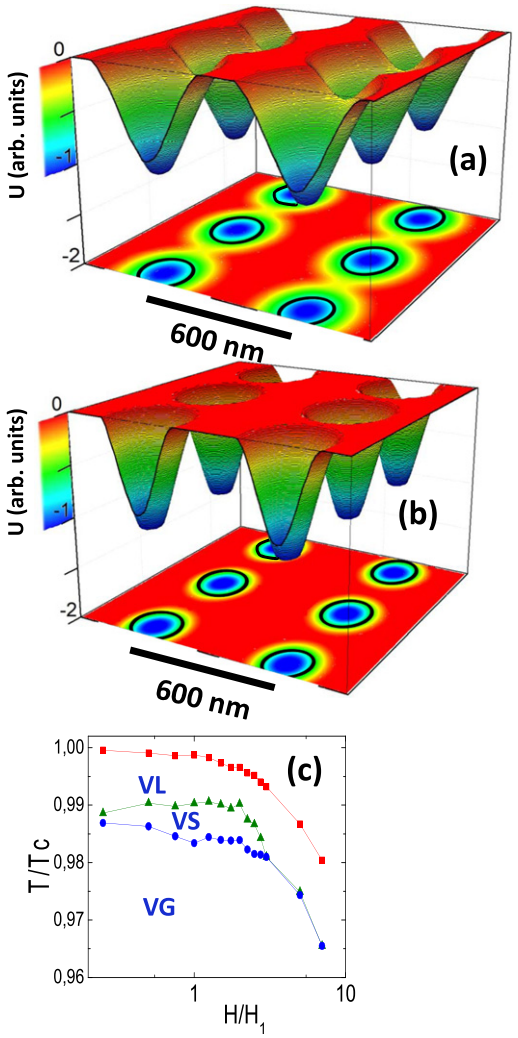

Figure 3. (a) Pinning potential (U) generated by sample R46 for $\xi = 95$ nm corresponding to $0.988\,T_c$. ξ being the coherence length. (b) Pinning potential (U) generated by sample R46 for $\xi = 70$ nm corresponding to $0.980\,T_c$. (c) Phase diagram (T, H) y-axis: T_c (red squares), $T_{g,l}$ (green triangles) and $T_{g,s}$ (blue dots). X-axis H/H_1 in log scale, H_1 being the first matching field. VL (vortex liquid), VS (vortex smectic) and VG (vortex glass) see text.

short or long sides of the array unit cell are $\nu_{\text{short}} = 1.1 \pm 0.1$, $z_{\text{short}} = 7.0 \pm 0.2$ and $\nu_{\text{long}} = 1.1 \pm 0.1$, $z_{\text{long}} = 5.5 \pm 0.2$ respectively. Therefore, we are dealing with an anisotropic vortex glass–to–vortex liquid melting transition [45, 46] in the high applied magnetic field region.

We can clarify this complex picture by studying how resistivity changes in a transition from the vortex liquid into a vortex smectic or glass phase (see [25, 45–47]). In both cases, close to the transition the resistivity drops to zero as a power law, i.e.

$$\rho \sim \left(T/T_g - 1\right)^{\mathbf{s}} \tag{2}$$

The critical exponent **s** can be obtained in a direct way: dividing ρ by its derivative $\delta\rho/\delta T$ and finding the slope of the resulting curve (see the inset of figure 5 for sample R46). In particular, for a vortex liquid-to-glass transition Equation (2) can be derived from Equation (1), and this critical exponent will be $\mathbf{s} = \nu(z + 2\text{-}D)$ [48, 49]. In that case the expected **s** values could be $3 \leqslant \mathbf{s} \leqslant 12$, taking into account $D = 3$ and the limits for both exponents ($\nu \approx 1$–2 and $z \approx 4$–7). The control sample SQ was measured and analyzed for several matching fields. In figure 5 we can see that the extracted **s** values are between 5 and 6, in the range expected for a vortex liquid to glass transition, and they do not depend on the magnetic field.

In the case of the 2-fold symmetry samples (R46 and R48), resistivity also follows equation (2) (see inset in figure 5) and the critical exponent **s** can be estimated. Figure 5 shows the results for both samples with selected applied magnetic fields which are fractions and multiples of the first matching fields. The **s** exponents show values that depend on the matching fields and they are lower than in the case of the control sample (SQ sample). We can notice two regimes: (i) the exponents **s** are less than 3 for matching fields lower than H_3. These low values

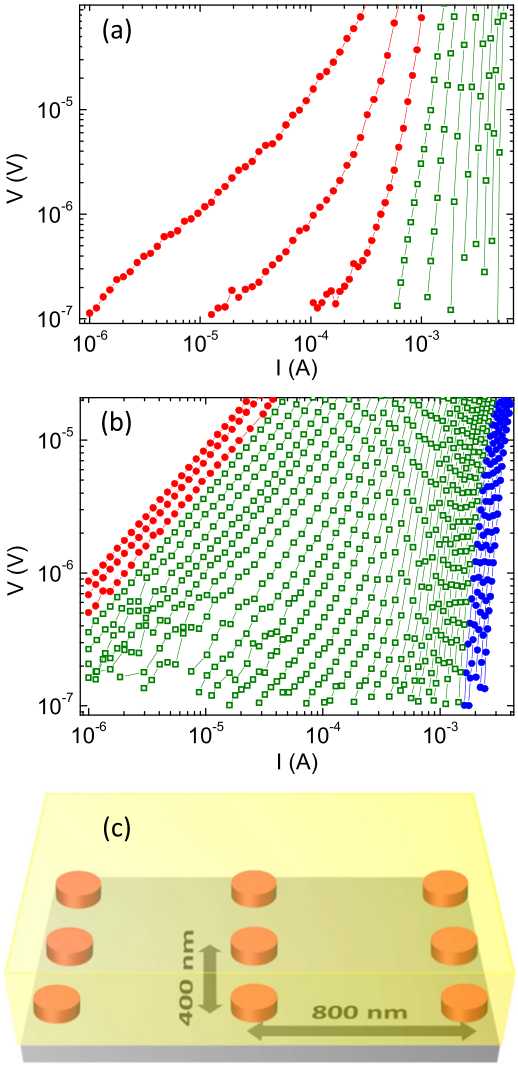

Figure 4. *I-V* isotherms for sample R48 ($T_c = 8.3$ K) data taken every 10 mK with $H = 63$ Oe ($H = H_1$): (a) from 0.988 T_c to T_c, vortices move along the long side of the rectangular array; (b) from 0.959 T_c to T_c vortices move along the short side of the rectangular array. $T_{gl} = 0.997$ T_c and $T_{gs} = 0.967$ T_c. Green hollow squares show the experimental data which spans between the vortex glass (blue dots) and vortex liquid (red dots). (c) Sketch of sample R48: array of Cu dots with 400 × 800 nm^2 unit cell embedded in Nb film grown on Si substrate. (Sketch is not to scale).

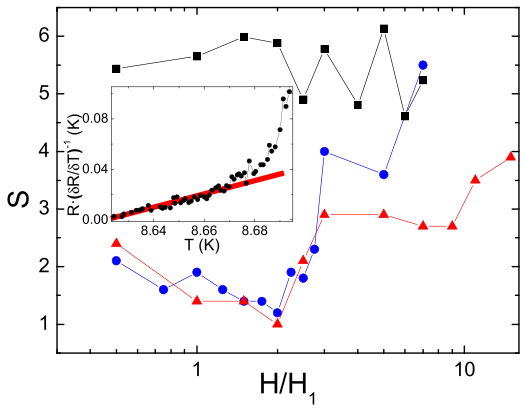

Figure 5. *Y*-axis critical exponent **s**, *x*-axis H/H_1 in log scale, H_1 being the first matching field for all samples. Sample SQ (black squares) and samples R46 (blue circles) and R48 (red triangles). The lines are guides to the eye. In the inset, linear fit to obtain **s**, as an example in sample 46. Resistivity drops as $(T\text{-}T_g)^{\mathbf{s}}$.

of **s** have been reported previously for smectic phases [4, 25, 47, 50]. (ii) For matching fields higher than $n = 3$, the critical exponent **s** rises, reaching, at the end, values that are between the expected values in the usual vortex glass–vortex liquid transition. Below the crossover (low applied magnetic field regime) the behavior of both samples looks similar, and above the crossover (high applied magnetic field regime) the samples behave differently. Sample R48 shows lower values and flatter behavior than sample R46. Recall that sample R48 shows an anisotropic scaling. In this case, the exponent values are in the lower limit of the expected values for the solid-to-liquid transition; i.e. the transition is smoother than usual, and the resistivity within the vortex liquid state drops to zero as a power law with lower exponents, i.e. less abruptly than the isotropic transition.

Finally, concerning the crossover, we have to address two experimental facts: the smectic phase is only observed for small applied magnetic fields, and this happens around the same magnetic field (around $3H_1$) in both samples. The interplay between potential landscapes and vortices could be a hint to explain these two results. First of all, an increase in the number of vortices in the array unit cell smears out the vortex-nanocenter interaction; for example, the matching field of $3H_1$ means one trapped vortex and two interstitial vortices per unit cell, hence the vortex lattice–pinning potential interaction is weaker than in the cases of H_1 (only trapped vortices) and $2H_1$ (trapped vortices and only one interstitial vortex). In conclusion, the weakness of the vortex–pinning landscape interaction precludes the smectic phase and the liquid phase is promoted. On the other hand, a comparison between samples R48 and R46 shows that the translation periodicity along the long side is distinct in each sample, but in the perpendicular direction the same potential landscape (400 nm between Cu dots) is found for both samples. Therefore, both samples look alike from this point of view. This could be the clue for finding a crossover at similar matching fields, since vortices probe the same potential landscape when they move along the short side of the rectangular unit cell.

4. Conclusions

In summary, plain superconducting Nb films can show an (H, T) phase diagram with a smectic region between the liquid and the solid phases. This is realized when the films are grown on top of an array of symmetric pinning centers. Interestingly, smectic order is achieved when the symmetry of the array is reduced from four-fold to two-fold. That is, in these non-layered superconductors, vortex matter shows a liquid-like or solid-like behavior depending on the vortex motion direction. This potential landscape is fabricated with a two-fold symmetric array of Cu nanodots embedded in the superconductor. The smectic phase is controlled by the array shape, temperature, and applied magnetic field. Finally, this smectic phase always vanishes when the number of vortices increases, and the usual vortex phase diagram is recovered with a vortex glass–to–vortex liquid crossover.

We thank Spanish MINECO grant FIS2013-45469 and CM grant S2013/MIT-2850 and EU COST Action MP-1201. D.G. acknowledges RYC-2012-09864.

References

[1] Hamon C, Novikov S, Scarabelli L, Basabe-Desmonts L and Liz-Marzan L M 2014 *ASC Nano* **8** 10694
[2] Mesaros A, Fujita K, Eisaki H, Uchida S, Davis J C, Sachdev S, Zaanen J, Lawler M J and Kim E A 2011 *Science* **333** 426
[3] Reddy R A *et al* 2011 *Science* **332** 72
[4] de Gennes P G 1972 *Solid State Commun.* **10** 753
[5] Carlson E W, Castro Neto A H and Campbell D K D K 2003 *Phys. Rev. Lett.* **90** 087001
[6] Reichhardt C and Olson Reichhardt C J 2006 *Europhys. Lett.* **75** 489
[7] Koselev A E and Vinokur V M 1994 *Phys. Rev. Lett.* **73** 3580
[8] Olson C J, Reichhardt C and Nori F 1998 *Phys. Rev. Lett.* **81** 3757
[9] Giarmarchi T and Le Doussal P 1998 *Phys. Rev.* B **57** 11356
[10] Tsuboi T, Hanaguri T and Maeda A 1998 *Phys. Rev. Lett.* **80** 4550
[11] Reichhardt C and Zimanyi G T 2000 *Phys. Rev.* B **61** 14354
[12] Reichhardt C and Reichhardt C J O 2012 *J. Phys. Condens. Matter* **22** 225702
[13] Wilson J A, Di Salvo F J and Majahan S 1975 *Adv. Phys.* **24** 117
[14] Vicent J L, Hillenius S J and Coleman R V R V 1980 *Phys. Rev. Lett.* **44** 892
[15] Xiao Z L, Andrei E Y and Higgins M J 1999 *Phys. Rev. Lett.* **83** 1664
[16] Bishop D J, Gammel P L, Huse D A and Murray C A 1992 *Science* **255** 165
[17] Blatter G, Feilg'man M M, Geshkenbein V B, Larkin A I and Vinokur V M 1994 *Rev. Mod. Phys.* **66** 1125
[18] Balents L and Nelson D R 1995 *Phys. Rev.* B **52** 12951
[19] Stewart G R 2011 *Rev. Mod. Phys.* **83** 1589
[20] Shein I R and Ivanovskii A L 2009 *Phys. Rev.* B **79** 245115
[21] Fernandes R M, Abrahams E and Schmalian J 2011 *Phys. Rev. Lett.* **107** 217002
[22] Blatter G, Ivlev B I and Rhyner J 1991 *Phys. Rev. Lett.* **66** 2392
[23] Giarmarchi T and Le Doussal P 1996 *Phys. Rev. Lett.* **76** 3408
[24] Balents L, Marchetti C M and Radzihovsky L 1997 *Phys. Rev. Lett.* **78** 75
[25] Kwok W K, Fendrich J, Welp U, Fleshler S, Downey J and Crabtree G W 1994 *Phys. Rev. Lett.* **72** 1088
[26] Pardo F, de la Cruz F, Gammel P L, Bucher E and Bishop D J D J 1998 *Nature* **396** 348

[27] Gordeev S N, Zhukov A A, de Groot P A J, Jansen A G M, Gagnon R and Taillefer L 2000 *Phys. Rev. Lett.* **85** 4594
[28] Harada K, Kamimura O, Kasai H, Matsuda T, Tonomura A and Moshchalkov V V 1996 *Science* **274** 1167
[29] Hoffmann A, Prieto P and Schuller I K 2000 *Phys. Rev.* B **61** 6958
[30] Villegas J E, Savelev S, Nori F, Gonzalez E M, Anguita J V, Garcia R and Vicent J L 2003 *Science* **302** 1188
[31] Milosevic M V and Peeters F M 2004 *Phys. Rev. Lett.* **93** 267006
[32] Perez de Lara D, Alija A, Gonzalez E M, Velez M, Martin J I and Vicent J L 2010 *Phys. Rev.* B **82** 174503
[33] Grimaldi G, Leo A, Nigro A, Silhanek A V, Verellen N, Moshchalkov V V, Milosevic M V, Casaburi A, Cristiano R and Pace S 2012 *Appl. Phys. Lett.* **100** 202601
[34] Volodin A, Temst K, Van Haesendonck C, Bruynseraede Y, Montero M I and Schuller I K 2002 *Europhys. Lett.* **58** 582
[35] Velez M, Jaque D, Martín J I, Guinea F and Vicent J L 2002 *Phys. Rev.* B **65** 094509
[36] Dinis L, Perez de Lara D, Gonzalez E M, Anguita J V, Parrondo J M R and Vicent J L 2009 *New J. Phys.* **11** 073046
[37] Pogosov W V, Misko V R, Zhao H J and Peeters F M 2009 *Phys. Rev.* B **79** 014504
[38] Kein T, Joumard I, Blanchard S, Marcus J, Cubitt R, Giamarchi T and Le Doussal P 2001 *Nature* **413** 404
[39] Gomez A, Gonzalez E M and Vicent J L 2012 *Supercond. Sci. Technol.* **25** 124006
[40] Fisher D S, Fisher M P A and Huse D A 1991 *Phys. Rev.* B **43** 130
[41] Strachan D R, Sullivan M C, Fournier P, Pai S P, Venkatesan T and Lobb C J 2001 *Phys. Rev.* B **87** 067007
[42] Villegas J E, Gonzalez E M, Sefrioui Z, Santamaria J and Vicent J L 2005 *Phys. Rev.* B **72** 174512
[43] Velez M, Jaque D, Martín J I, Montero M I, Schuller I K and Vicent J L 2002 *Phys. Rev.* B **65** 104511
[44] Campbell A M and Evetts J E 2011 *Adv. Phys.* **50** 1249
[45] Kotzler J, Kaufmann M, Nakielski G, Behr R and Assmus W 1994 *Phys. Rev. Lett.* **72** 2081
[46] Espinosa-Arronte B, Andersson M, van der Beek C J, Nikolaou M, Lidmar J and Wallin M 2007 *Phys. Rev.* B **75** 100504(R)
[47] Baily S A, Maiorov B, Zhou H, Balakirev F F, Jaime M, Foltyn S R and Civale L 2008 *Phys. Rev. Lett.* **100** 027004
[48] Reed D S, Yeh N C, Jiang W, Kriplani U and Holtzberg F 1993 *Phys. Rev.* B **47** 6150
[49] Yamasaki H, Endo K, Kosaka S, Umeda M, Yoshida S and Kajimura K 1994 *Phys. Rev.* B **50** 12959
[50] Nelson D R and Vinokur V M 1993 *Phys. Rev.* B **48** 13060